

## Viscous Entrainment from a Nozzle: Singular Liquid Spouts

Wendy W. Zhang

*The Physics Department & James Franck Institute, University of Chicago, Chicago, Illinois 60637, USA*  
(Received 5 January 2004; published 28 October 2004)

We analyze a long-wavelength model of viscous entrainment from a nozzle and show that, when appropriate large-scale boundary conditions are imposed, the entrainment transition can become continuous. As the entrainment threshold is approached from above, the entrained steady-state spout becomes vanishingly thin compared to the nozzle radius and takes the form of a thin tendril emerging from a base profile whose tip is perfectly conical.

DOI: 10.1103/PhysRevLett.93.184502

PACS numbers: 47.55.Dz, 47.20.Gv, 47.20.Ky, 47.54.+r

A small air bubble rising in syrup remains entire while a larger air bubble can be so severely deformed by the rising movement that air is entrained from the bubble. Recently, Cohen and Nagel examined an analogous transition by using flow in an upper layer of viscous oil to entrain water from a lower layer [1,2]. Focusing on the dynamics as the entrainment threshold is approached from below, they found that the steady-state water-oil interface develops a near cusp. The entrainment transition is mediated via steady-state shapes until the cusp reaches a cutoff length of  $10\ \mu\text{m}$ . Experiments with different fluid pairs, even pairs of comparable viscosities, show basically the same weakly discontinuous transition, with similar values for the cutoff length.

Here we ask whether it is possible for the entrainment transition to be continuous, mediated entirely via steady-state shapes. We focus on the dynamics as the entrainment transition is approached from above, a scenario relevant for potential technological applications, e.g., encapsulation of Islet of Langerhans [3] and flow focusing [4]. We found that, provided the large-scale shape of the interface assumes a particular form, a vanishingly thin, steady-state spout is created as the entrainment threshold is approached from above.

To see why this might be so, note that the formation of a vanishingly thin spout at the entrainment threshold requires essentially that the dynamics on the shortest length scale decouple completely from the dynamics on other length scales. For such a transition to occur via steady-state shapes, this decoupling must occur without a concomitant separation of time scales, in contrast to transitions via finite-time singularities, e.g., surface-tension driven breakup of a liquid drop [5–7], where the time scales and the length scales can both separate. In a steady-state transition, the smallest length scale can shrink to 0 if and only if such a shrinkage is consistent with the dynamics on all larger length scales. This is why a vanishingly thin spout forms at the viscous entrainment transition only for appropriate boundary conditions on the large-scale interface shape.

To work this idea out in detail, we devised a particularly simple entrainment problem (Fig. 1). Fluid of vis-

cosity  $\mu_0$  is entrained from a nozzle with radius  $a$  by an axisymmetric straining flow,  $(-Er/2, 0, Ez)$ , in the exterior fluid, which has viscosity  $\mu$ . The stagnation point of the imposed straining flow is also the origin of our cylindrical coordinate system. The nozzle is connected to a fluid reservoir. At the nozzle opening  $z_N$ , the spout has the same radius as the nozzle and its contact angle is  $\theta_N$ . Following Taylor's and others' studies on drop emulsification [8,9], we focus on the limit  $\mu_0 \ll \mu$ , where the coupling between the induced interior flow and the imposed exterior flow simplifies to a balance between the interior pressure  $P_0$  and the exterior viscous stress  $\mu E$ . For a spout of radius  $R$  and axial length scale  $d$ , the interior pressure gradient  $P_0/d$  is roughly  $\mu_0(Ed)/R^2$ . Requiring  $P_0 \approx \mu E$  then yields  $R/d \propto \sqrt{\mu_0/\mu}$ . This scaling for the aspect ratio of the entrained spout,  $R/d$ , suggests that, provided  $\theta_N$  is close to  $90^\circ$  so that  $dR/dz(z_N) \ll 1$ , the spout slope  $dR/dz$  is everywhere small. The entrainment dynamics is accurately described by a long-wavelength model, even near the entrainment transition. To take full advantage of this possible simplification, we require that, in the model problem, the pres-

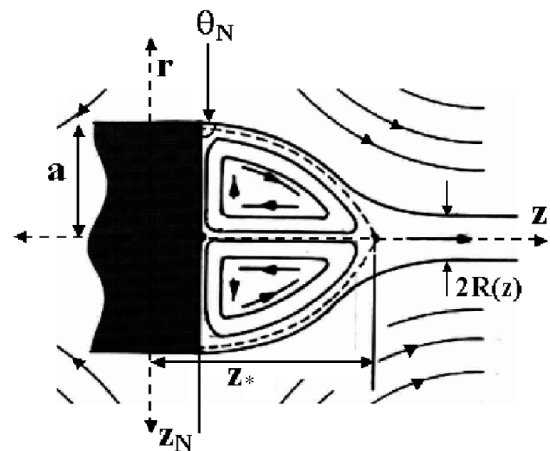


FIG. 1. An axisymmetric straining flow  $(-Er/2, 0, Ez)$  in the exterior fluid entrains an immiscible fluid from a nozzle located at  $z_N$ . The entrained, steady-state spout has radius  $R(z)$  and contact angle  $\theta_N$  at the nozzle.

sure in the reservoir connected to the nozzle is adjusted for each flow rate so that  $\theta_N$  has the same value for all  $E$ .

Before presenting quantitative results, we give a qualitative description of a continuous entrainment transition. When  $\mu_0 \ll \mu$ , entrainment ceases when the exterior viscous stress is smaller than surface-tension pressure  $\gamma/a$ , where  $\gamma$  is surface tension, so the entrainment threshold  $E_c$  scales as  $\gamma/(\mu a)$ . Below  $E_c$ , no fluid is entrained and the interior flow is a toroidal eddy with a stagnation point at the tip of the extended interface. Just above  $E_c$ , the same picture holds except for one important difference: the stagnation point  $z_*$  now lies inside the entrained spout (Fig. 1). Thus, as  $E$  approaches  $E_c$  from above, a continuous entrainment transition corresponds to a smooth evolution of the location of the stagnation point from the interior of the entrained spout onto the interface.

To see how such a smooth evolution in  $z_*$  location comes about, consider momentum balance near  $z_*$ . The spout shape near  $z_*$  is characterized by the radius  $R_* = R(z_*)$  and axial length scale  $d_* = 1/[d^2R/dz^2(z_*)]$ . In the momentum balance, these length scales determine the relative sizes of the viscous forcing from the exterior flow,  $\mu U_*/R_*^2$ , where  $U_* = Ez_*$  is the exterior velocity at  $z_*$ , the viscous resistance from the interior flow,  $\mu_0 U_*/R_*^2$ , and the surface-tension pressure gradient  $\gamma/(R_* d_*)$ . All three effects diverge as  $R_*$  goes to 0. For the entrained spout to continue to exist as  $E$  approaches  $E_c$ , these three terms must at least diverge with the same pace, so that the form of the momentum balance is unchanged. This is possible if

$$d_* \propto R_*, \quad (1)$$

corresponding to a base shape which develops a perfectly conical tip at  $z_*$  as  $E$  approaches  $E_c$ . This is the base shape necessary for a continuous entrainment transition to take place. Otherwise, the form of the local momentum balance will change as  $R_*$  decreases, thereby cutting off the decrease in  $R_*$ .

Since  $R_*$  and  $d_*$  are shaped by the flow and cannot be directly imposed via boundary conditions, it is unclear whether the entrained spout would ever converge onto the desired shape (1). We therefore turn to an analysis of the long-wavelength model. In the analysis, we use nondimensional variables where radial length scales are rescaled by the nozzle radius  $a$ , axial length scales by  $a\sqrt{\mu/(4\mu_0)}$ , and various fluid stresses and pressures by  $\gamma/a$ . Conservation of volume flux  $Q$  inside the spout gives us an equation for the dimensionless steady-state spout  $R(z)$ ,

$$Q = \int_S U_0(z, r) dS = zCaR^2(z) - R^4(z)(dP_0/dz), \quad (2)$$

where  $U_0(z, r)$  is the interior axial velocity,  $S(z)$  is the cross-sectional area of the spout, and  $Ca = (2\mu Ea)/\gamma$ , a ratio of exterior viscous stress over surface-tension pressure, is the dimensionless strain rate. The interior volume

flux  $Q$  has one contribution from an interior plug flow induced by the exterior flow and another contribution from a Poiseuille flow driven by the interior pressure,  $P_0(z) = (1/R) - 4(\mu_0/\mu)(d^2R/dz^2) + Ca(z/R)(dR/dz)$ . The pressure contains contributions from surface tension (radial and axial curvature), and exterior viscous stress [10]. Equation (2) is solved with the boundary conditions  $R(z_N) = 1$  and  $dR/dz(z_N) = \sqrt{\mu/4\mu_0} \cot(\theta_N)$  at the nozzle opening  $z_N$  and, far downstream, the entrainment condition  $R(z) \rightarrow \sqrt{Q/(zCa)}$  as  $z \rightarrow \infty$ . For a given  $Ca$ , these boundary conditions uniquely determine  $Q$  and  $R(z)$  [11].

We next simplify Eq. (2) further by assuming that, for a vanishingly thin steady-state spout to form, the dynamics in the vicinity of  $z_*$  must become scale invariant, governed solely by how closely  $Q$  approaches 0. Entrainment dynamics at different values of  $Q$  should appear identical when  $r$  and  $z$  axes are appropriately rescaled by  $Q$ . We already know from local momentum balance (1) that  $d_* \propto R_*$ . From volume flux conservation  $Q \approx U_* \pi R_*^2$ , we see also that  $R_* \propto \sqrt{Q}$ . We therefore conclude that a scale-invariant spout must have the form

$$R(z) = \sqrt{Q}\rho(\eta) \quad \eta = (z - z_*)/\sqrt{Q}. \quad (3)$$

Substituting (3) into Eq. (2) and taking the limit  $Q \rightarrow 0$  yield

$$1 = U_* \rho^2 - \rho^4 \frac{d}{d\eta} \left\{ \left[ \frac{1}{\rho} - 4 \left( \frac{\mu_0}{\mu} \right) \frac{d^2 \rho}{d\eta^2} \right] + \frac{U_*}{\rho} \frac{d\rho}{d\eta} \right\}, \quad (4)$$

an equation for the scale-invariant spout profile. Downstream, the entrainment condition simplifies to  $\rho(\eta) \rightarrow \sqrt{1/U_*}$  as  $\eta \rightarrow \infty$ , because in the rescaled coordinates the entrained tendril appears cylindrical. Upstream, the separation of length scale means the nozzle boundary conditions are irrelevant. Instead, motivated by (1), we require  $\rho(\eta) \propto s\eta$  as  $\eta \rightarrow -\infty$ , which corresponds to looking for an upstream shape consistent with the assumption of scale invariance. Starting far downstream with the desired  $\sqrt{1/U_*}$  entrained tendril and numerically integrating (4) backwards via a standard shooting scheme, we found that Eq. (4) supports an entire family of scale-invariant spout solutions, parametrized by the exterior entrainment velocity  $U_*$ . More precisely, for  $U_*$  below a maximum value of  $U_*^{\max} = 1/2$ , two conical base profiles are possible for every  $U_*$ , with cone slopes  $s_{\pm} = [(-1/U_*) \pm \sqrt{(1/U_*^2) - 4}]/2$ . Of the two cones, the entrained cylindrical tendril always emerges from the smaller cone, while the larger cone is connected to a solution which blows up at finite  $\eta$ , as illustrated in Fig. 2.

We next show that the full entrainment dynamics, as described by (2), converges onto the scale-invariant dynamics described by (4) when nozzle boundary conditions have appropriate values. This task typically requires

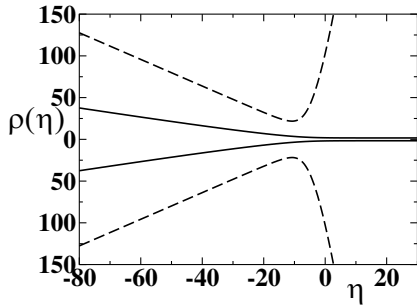


FIG. 2. Scale-invariant spout solution (solid line) for  $U_* = 0.45$  showing the entrained cylindrical tendril emerging from the smaller cone. The larger cone (dashed line) gives rise to a solution which blows up at finite  $\eta$ . ( $\mu_0/\mu = 1/80$ .)

solving (2) numerically for different values of  $z_N$  and  $dR/dz(z_N)$ , in essence mapping out the region of appropriate values by conducting a sweep across the entire phase plane (Fig. 3). Our model entrainment problem, however, allows a shortcut. We know that, at the threshold of a continuous entrainment transition, the spout base shape must approach a  $Q = 0$  solution of (2). For the dynamics near  $z_*$  to be scale invariant, this  $Q = 0$  shape must have a perfectly conical tip at  $z_*$  with  $U_* < U_*^{\max}$ . We therefore look for a  $Q = 0$  solution of (2) in the form  $R(z) = 1 - (z/z_*)^2$ , the simplest polynomial which ends in a cone. Equation (2) turns out to support a family of exact solutions in precisely this form, with radius

$$H(z) = 1 - \left(\frac{z}{z_*}\right)^2 \quad z_* = 2\sqrt{\frac{1}{2Ca_c} - 1}. \quad (5)$$

Of these, the solutions with  $Ca_c < 1/4$  satisfy  $U_* < U_*^{\max}$ . These are large-scale spout shapes which support continuous entrainment transitions. Therefore, when the nozzle boundary condition has values  $R(z_N) = H(z_N, Ca_c)$  and  $dR/dz(z_N) = dH/dz(z_N, Ca_c)$  with  $Ca_c \leq 1/4$ , as indicated on the phase diagram in Fig. 3

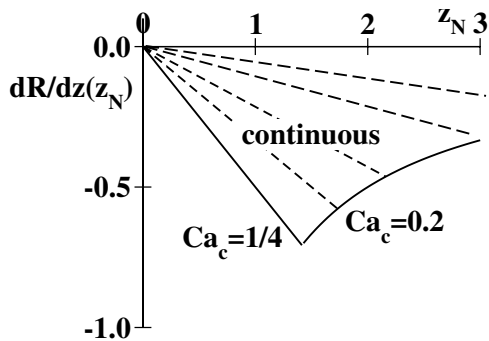


FIG. 3. Phase diagram with horizontal axis  $z_N$ , the nozzle location, and vertical axis  $dR/dz(z_N) = \sqrt{\mu/(4\mu_0)} \cot\theta_N$ . Values corresponding to entrainment transition at one particular  $Ca_c$  lie on a line segment (dashed lines).

[12], a continuous entrainment transition should take place at  $Ca = Ca_c$ .

Numerical solutions of Eq. (2) confirm that, when the boundary conditions at the nozzle have values which lie inside the continuous transition parameter region, a vanishingly thin, steady-state spout is created at the transition. When nozzle boundary condition values lie outside the region, the steady-state entrainment dynamics has either a cutoff in  $Q$  or no critical behavior at all (not shown here). Below we describe one calculated continuous entrainment transition in more detail. The calculation has nozzle opening  $z_N = 0.05$  and the nozzle boundary conditions with  $Ca_c = 0.2$ . The steady-state spout solutions were obtained by starting with  $Ca = 2$  and then using Newton relaxation to solve for solutions at successively smaller values of  $Ca$  [13]. As can be seen from Fig. 4, the large-scale shape of the steady-state spout indeed converges onto  $H(z, Ca_c = 0.2)$  as  $Ca$  is decreased towards  $Ca_c$ , or equivalently, as  $Q$  decreases towards 0 (Fig. 5). The inset to Fig. 5 shows both  $R_*$  and  $d_*$  scale as  $\sqrt{Q}$ , which strongly suggests that the spout shape near  $z_*$  is converging towards a scale-invariant shape. We checked this idea rigorously by rescaling the steady-state spout shapes at  $Q = 10^{-2}, 10^{-3}$ , and  $10^{-5}$  via ansatz (3) and comparing the rescaled shapes against the scale-invariant solution at  $U_* = z_*(Ca_c)Ca_c$  for  $Ca_c = 0.2$ . Figure 6 displays the outcome. Not only do the rescaled full solutions collapse onto a single curve, but the collapsed curves also lie on top of the scale-invariant solution. This clearly shows that the entrainment dynamics is associated with a complete separation of length scales and hence a continuous transition. We emphasize that the agreement in Fig. 6 involves no fitting parameters because the  $z_*$  values used to shift the various shapes onto each other were calculated directly from the numerical solutions.

We believe the continuous entrainment transition found here can be realized in an experiment. Our calculation corresponds to an experimental protocol which is unusual but not impractical. Starting with a thick spout at

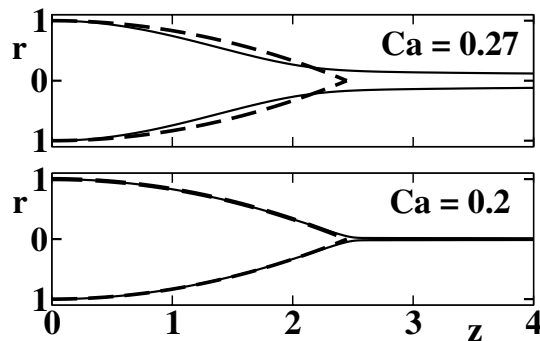


FIG. 4. Steady-state spout shape at dimensionless strain rate  $Ca = 0.27$  and  $Ca = Ca_c = 0.2$ . The dashed lines outline the  $Q = 0$  shape corresponding to  $H(z, Ca_c = 0.2)$ . The nozzle is located at  $z_N = 0.05$  and  $\mu_0/\mu = 1/80$ .

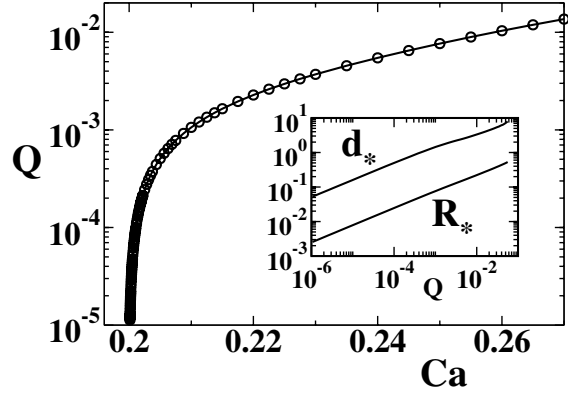


FIG. 5. Volume flux  $Q$  of the entrained fluid as a function of  $Ca$ . The inset shows the spout radius  $R_*$  and the axial length scale  $d_* = 1/[d^2R/dz^2(z_*)]$  decrease as  $\sqrt{Q}$  as  $Q$  goes to 0.

large  $E$ , we approach the entrainment threshold  $E_c$  by reducing  $E$  via successively smaller decrements so that the steady-state spout shape changes only quasistatically. We also require that the pressure conditions in the fluid reservoir are adjusted at every  $E$  so that the contact angle at the nozzle,  $\theta_N$ , has the same value for all  $E$ . While the second requirement is necessary for the long-wavelength analysis to remain relevant, as noted earlier, it is unclear whether it is necessary for the experimental realization. A second possible complication is the existence of time-dependent surface-tension driven instabilities which can prevent the steady-state spout from being realized in practice. Simple arguments suggest these are unlikely. Above  $z_*$ , where the spout looks most tenuous, it is being strongly stretched by the exterior straining flow and hence stable. Below  $z_*$ , the spout shape is maintained by surface tension and is again stable. At  $z_*$ , there is possible absolute instability when the surface-tension breakup velocity  $\gamma/\mu$  equals  $U_* \approx Ea\sqrt{\mu/\mu_0}$ . This occurs when  $Ca_c \approx \sqrt{\mu_0/\mu}$  so that, at least when  $\mu_0 \ll \mu$ , the entrained spout should always be stable.

Our analysis suggests that the weakly discontinuous entrainment transition observed by Cohen and Nagel results from the large-scale shape of the interface deviating only slightly from the shape consistent with a continuous transition, a possibility we plan to examine further.

In conclusion, we analyzed the steady-state entrainment dynamics in a model problem using a combination of scaling arguments, asymptotic analysis, and numerics. We showed that, when appropriate boundary conditions are imposed on the large-scale shape of the spout, a continuous entrainment transition takes place. Near such a transition, the entrained spout becomes vanishingly thin compared to the nozzle radius and takes the form of a thin tendril emerging from a base profile with a perfectly conical tip.

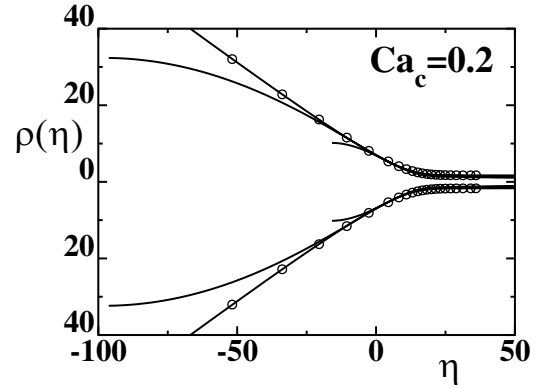


FIG. 6. Steady-state spout shapes (solid lines) with  $Q = 10^{-2}$ ,  $Q = 10^{-3}$ , and  $Q = 10^{-5}$  rescaled as  $\rho(\eta) = R(z)/\sqrt{Q}$  and  $\eta = (z - z_*)/\sqrt{Q}$  and compared against the scale-invariant solution (open circles, every 20th point shown).

I am grateful to Sidney R. Nagel, Michael P. Brenner, Itai Cohen, Todd F. Dupont, Jens Eggers, Alfonso Gañán-Calvo, Leo P. Kadanoff, David Quere, Howard A. Stone, Shankar Venkataramani, Thomas A. Witten, and Jason Wyman for insightful suggestions. This research is supported by the NSF (DMS-0102033) and by the Materials Research Science and Engineering Center at University of Chicago.

- 
- [1] I. Cohen and S.R. Nagel, Phys. Rev. Lett. **88**, 074501 (2002).
  - [2] I. Cohen, Phys. Rev. E **70**, 026302 (2004).
  - [3] I. Cohen, H. Li, J.L. Houglund, M. Mrksich, and S.R. Nagel, Science **292**, 265 (2001).
  - [4] A.M. Ganan-Calvo, Phys. Rev. Lett. **80**, 285 (1998).
  - [5] I. Cohen, M.P. Brenner, J. Eggers, and S.R. Nagel, Phys. Rev. Lett. **83**, 1147 (1999).
  - [6] W.W. Zhang and J.R. Lister, Phys. Rev. Lett. **83**, 1151 (1999).
  - [7] J. Eggers, Rev. Mod. Phys. **69**, 865 (1997).
  - [8] G.I. Taylor, in *Applied Mechanics: Proceedings of the 11th International Congress of Applied Mechanics, Munich, 1964* (Springer-Verlag, Berlin, New York, 1964), Vol. 11, p. 191.
  - [9] A. Arivos and T.S. Lo, J. Fluid Mech. **86**, 641 (1978).
  - [10] Though the axial curvature  $d^2R/dz^2$  is a higher order term than  $1/R$ , its presence is essential as it represents the physical mechanism by which short-wavelength disturbances are in reality smoothed out.
  - [11] For the same nozzle boundary conditions, other values of  $Q$  give rise to unphysical  $R(z)$  shapes, some of which terminate or blow up at finite  $z$ . Others bulge and contract along  $z$ .
  - [12] Figure 3 uses the rescaling convention  $H(z=0) = 1$ .
  - [13] To ensure that the small-scale structure in the neighborhood of  $z_*$  is properly resolved, we use a grid scheme whose spacing is weighted by the local axial curvature.